ECOLE POLYTECHNIQUE

CENTRE DE MATHÉMATIQUES APPLIQUÉES
UMR CNRS 7641

91128 PALAISEAU CEDEX (FRANCE). Tél: 01 69 33 41 50. Fax: 01 69 33 30 11

http://www.cmap.polytechnique.fr/

Structural optimization using sensitivity analysis and a level-set method

Grégoire ALLAIRE, François JOUVE,
Anca-Maria TOADER

R.I. N^0 508 *July 2003*

Structural optimization using sensitivity analysis and a level-set method

Grégoire ALLAIRE [*] François JOUVE [†]

Anca-Maria TOADER [‡]

July 2, 2003

Abstract

In the context of structural optimization we propose a new numerical method based on a combination of the classical shape derivative and of the level-set method for front propagation. We implement this method in two and three space dimensions for a model of linear or nonlinear elasticity. We consider various objective functions with weight and perimeter constraints. The shape derivative is computed by an adjoint method. The cost of our numerical algorithm is moderate since the shape is captured on a fixed Eulerian mesh. Although this method is not specifically designed for topology optimization, it can easily handle topology changes. However, the resulting optimal shape is strongly dependent on the initial guess.

Keywords: shape optimization , topology optimization , sensitivity analysis , shape derivative , level-set.

Acknowledgements. This work has been supported by the grant CNRS/GRICES n^o 2002-12163 of the Centre National de la Recherche Scientifique (France) and the Gabinete de Relações Internacionais da Ciência e do Ensino Superio (Portugal).

1 Introduction

Shape optimization of elastic structures is a very important and popular field. The classical method of shape sensitivity (or boundary variation) has been much studied (see e.g. [22], [25], [29], [31]). It is a very general method which can

[*] Centre de Mathématiques Appliquées (UMR 7641), Ecole Polytechnique, 91128 Palaiseau, France — gregoire.allaire@polytechnique.fr

[†] Centre de Mathématiques Appliquées (UMR 7641), Ecole Polytechnique, 91128 Palaiseau, France — francois.jouve@polytechnique.fr

[‡] CMAF, Faculdade de Ciências da Universidade de Lisboa, Av. Prof. Gama Pinto 2, 1699 Lisboa, Portugal — amtan@ptmat.fc.ul.pt

handle any type of objective functions and structural models, but it has two main drawbacks: its computational cost (because of remeshing) and its tendency to fall into local minima far away from global ones. The homogenization method (and its variants, such as power-law materials or SIMP method, see e.g. [1], [2], [5], [8], [9], [10], [17]) is an adequate remedy to these drawbacks but it is mainly restricted to linear elasticity and particular objective functions (compliance, eigenfrequency, or compliant mechanism). Recently yet another method appeared in [23], [27] based on the level-set method which has been devised by Osher and Sethian [24], [26] for numerically tracking fronts and free boundaries. The level-set method is versatile and computationally very efficient: it is by now a classical tool in many fields such as motion by mean curvature, fluid mechanics, image processing, etc.

The work [23] studied a two-phase optimization of a membrane (modeled by a linear scalar partial differential equation), i.e. the free boundary was the interface between two constituents occupying a given domain. It combined the level-set method with the shape sensitivity analysis framework. On the other hand, the work [27] focused on structural optimization within the context of two-dimensional linear elasticity. The shape of the structure was the free boundary which was captured on a fixed mesh using the immersed interface method. However, [27] did not rely on shape sensitivity analysis: rather the structural rigidity was improved by using an ad hoc criteria based on the Von Mises equivalent stress. Remark that the level-set method is close to another approach proposed in [11] and based on a phase-field model.

In this paper we generalize these two previous works in many aspects. We propose a systematic implementation of the level-set method where the front velocity is derived from a shape sensitivity analysis. We investigate different objective functions in two and three space dimensions: compliance (rigidity), least square deviation from a target (compliant mechanism), design dependent loads (pressure loads). Other objective functions like eigenfrequencies, multiple loads and minimal stress will be addressed in another paper. We focus on shape optimization rather than two-phase optimization, and we replace the immersed interface method by the simpler "ersatz material" approach which amounts to fill the holes by a weak phase. This is a well-known approach in topology optimization which can be rigorously justified in some cases [1]. We also consider the case of a nonlinear elasticity model. For all such problems we compute a shape derivative by using an adjoint problem. Then, the shape derivative is used as the normal velocity of the free boundary which is moved during the optimization process. Front propagation is performed by solving a Hamilton-Jacobi equation for a level-set function. We study the effect of first-order or second-order discretization and of reinitialization in the numerical convergence toward an optimal shape. We also investigate the strong dependence of the computed optimal shape on the initial design. Our results were announced in [4]. Related results have been independently obtained in [32].

2 Setting of the problem

We start by describing a model problem in linearized elasticity. There is no conceptual difficulty in choosing another model, and in particular Section 8 deals with a nonlinear elasticity problem. Let $\Omega \subset \mathbb{R}^d$ ($d = 2$ or 3) be a bounded open set occupied by a linear isotropic elastic material with Hooke's law A. Recall that, for any symmetric matrix ξ, A is defined by

$$A\xi = 2\mu\xi + \lambda\big(\mathrm{Tr}\xi\big)\,\mathrm{Id},$$

where μ and λ are the Lamé moduli of the material. The boundary of Ω is made of two disjoint parts

$$\partial\Omega = \Gamma_N \cup \Gamma_D, \tag{1}$$

with Dirichlet boundary conditions on Γ_D, and Neumann boundary conditions on Γ_N. The two boundary parts Γ_D and Γ_N are allowed to vary in the optimization process, although it is possible to fix some portion of it (see the numerical examples below).

We denote by f the vector-valued function of the volume forces and by g that of the surface loads. The displacement field u in Ω is the solution of the linearized elasticity system

$$\left\{\begin{array}{rcll} -\mathrm{div}\,(A\,e(u)) & = & f & \text{in } \Omega \\ u & = & 0 & \text{on } \Gamma_D \\ \big(A\,e(u)\big)n & = & g & \text{on } \Gamma_N. \end{array}\right. \tag{2}$$

Since Ω is varying during the optimization process, f and g must be known for all possible configurations of Ω. We therefore introduce a working domain D (a bounded open set of $\mathbb{R}^d$) which contains all admissible shapes Ω.

To give a precise mathematical meaning to (2), we choose $f \in L^2(D)^d$ and $g \in H^1(D)^d$ and we assume that $\Gamma_D \neq \emptyset$ (otherwise we should impose an equilibrium condition on f and g). In such a case it is well known that (2) admits a unique solution in $H^1(\Omega)^d$.

The objective function is denoted by $J(\Omega)$. In this paper, we shall mostly focus on two possible choices of J (these are merely examples, and much more freedom is allowed). A first classical choice is the compliance (the work done by the load)

$$J_1(\Omega) = \int_\Omega f\cdot u\,dx + \int_{\Gamma_N} g\cdot u\,ds = \int_\Omega A\,e(u)\cdot e(u)\,dx, \tag{3}$$

which is very common in rigidity maximization. A second choice is a least square error compared to a target displacement

$$J_2(\Omega) = \left(\int_\Omega k(x)|u-u_0|^\alpha dx\right)^{1/\alpha}, \tag{4}$$

which is a useful criterion for the design of compliant mechanisms [3], [28]. We assume $\alpha \geq 2$, $u_0 \in L^\alpha(D)$ and $k \in L^\infty(D)$, a non-negative given weighting factor. In both formulas (3) and (4), $u = u(\Omega)$ is the solution of (2). We define a set of admissible shapes that must be open sets contained in the working domain D and of fixed volume V

$$\mathcal{U}_{ad} = \Big\{ \Omega \subset D \text{ such that } |\Omega| = V \Big\}. \tag{5}$$

Our model problem of shape optimization is

$$\inf_{\Omega \in \mathcal{U}_{ad}} J(\Omega). \tag{6}$$

It is well known that the minimization problem (6) is usually not well posed on the set of admissible shapes defined by (5) (i.e. it has no solution). In order to obtain existence of optimal shapes some smoothness or geometrical or topological constraints are required. For example, a variant of (6) with a perimeter constraint turns out to be a well-posed problem (see [6]). The perimeter $P(\Omega)$ of an open set Ω is defined as the $(d-1)$-dimensional Hausdorff measure of its boundary $\partial\Omega$, i.e. $P(\Omega) = \mathcal{H}^{d-1}(\partial\Omega)$, which reduces to $P(\Omega) = \int_{\partial\Omega} ds$ for smooth domains. Then, if $\ell > 0$ is a positive Lagrange multiplier, the minimization problem

$$\inf_{\Omega \in \mathcal{U}_{ad}} \Big(J(\Omega) + \ell P(\Omega) \Big) \tag{7}$$

admits at least one optimal solution. There are other regularized variants of (6) which are well-posed and we refer to [13], [16] for such existence theories. Note that, even if existence is not an issue of the present paper, we shall work with a smoother subset of (5) in order to define properly a notion of shape derivative.

Remark 2.1. *We described our shape optimization problem with a single state equation, i.e. the shape is optimized for a single set of loads. Our approach can easily be generalized to the more meaningful case of shape optimization for multiple loads.*

3 Shape derivative

In order to apply a gradient method to the minimization of (6) we recall a classical notion of shape derivative. This notion goes back, at least, to Hadamard, and many have contributed to its development (see e.g. the reference books [25], [31]). Here, we follow the approach of Murat and Simon [22], [29]. Starting from a smooth reference open set Ω, we consider domains of the type

$$\Omega_\theta = \big(\mathrm{Id} + \theta \big)(\Omega),$$

with $\theta \in W^{1,\infty}(\mathbb{R}^d, \mathbb{R}^d)$. It is well known that, for sufficiently small θ, $(\mathrm{Id} + \theta)$ is a diffeomorphism in $\mathbb{R}^d$.

Definition 3.1. *The shape derivative of $J(\Omega)$ at Ω is defined as the Fréchet derivative in $W^{1,\infty}(\mathbb{R}^d,\mathbb{R}^d)$ at 0 of the application $\theta \to J\big((\mathrm{Id}+\theta)(\Omega)\big)$, i.e.*

$$J\big((\mathrm{Id}+\theta)(\Omega)\big) = J(\Omega) + J'(\Omega)(\theta) + o(\theta) \quad \textit{with} \quad \lim_{\theta\to 0} \frac{|o(\theta)|}{\|\theta\|} = 0\ ,$$

where $J'(\Omega)$ is a continuous linear form on $W^{1,\infty}(\mathbb{R}^d,\mathbb{R}^d)$.

A classical result states that the directional derivative $J'(\Omega)(\theta)$ depends only on the normal trace $\theta\cdot n$ on the boundary $\partial\Omega$.

Lemma 3.2. *Let Ω be a smooth bounded open set and $J(\Omega)$ a differentiable function at Ω. Its derivative satisfies*

$$J'(\Omega)(\theta_1) = J'(\Omega)(\theta_2)$$

if $\theta_1,\theta_2 \in W^{1,\infty}(\mathbb{R}^d;\mathbb{R}^d)$ are such that $\theta_2-\theta_1 \in \mathcal{C}^1(\mathbb{R}^d;\mathbb{R}^d)$ and

$$\theta_1\cdot n = \theta_2\cdot n \qquad \textit{on } \partial\Omega.$$

We give two examples of shape derivative that will be useful in the sequel.

Lemma 3.3. *Let Ω be a smooth bounded open set and $\phi(x)\in W^{1,1}(\mathbb{R}^d)$. Define*

$$J(\Omega) = \int_\Omega \phi(x)\,dx.$$

Then J is differentiable at Ω and

$$J'(\Omega)(\theta) = \int_\Omega \mathrm{div}\big(\theta(x)\,\phi(x)\big)\,dx = \int_{\partial\Omega} \theta(x)\cdot n(x)\,\phi(x)\,ds$$

for any $\theta\in W^{1,\infty}(\mathbb{R}^d;\mathbb{R}^d)$.

Lemma 3.4. *Let Ω be a smooth bounded open set and $\phi(x)\in W^{2,1}(\mathbb{R}^d)$. Define*

$$J(\Omega) = \int_{\partial\Omega} \phi(x)\,ds.$$

Then J is differentiable at Ω and

$$J'(\Omega)(\theta) = \int_{\partial\Omega} \theta\cdot n\left(\frac{\partial\phi}{\partial n} + H\phi\right) ds,$$

for any $\theta\in W^{1,\infty}(\mathbb{R}^d;\mathbb{R}^d)$, where H is the mean curvature of $\partial\Omega$ defined by $H=\mathrm{div} n$. Furthermore, this result still holds true if one replaces $\partial\Omega$ by Γ, a smooth open subset of $\partial\Omega$, and assumes that $f=0$ on the surface boundary $\partial\Gamma$.

Remark 3.5. *In particular Lemma 3.3 is useful in order to compute the shape derivative of a volume constraint $V(\Omega) = C$. Indeed, we have*

$$V(\Omega) = \int_\Omega dx \quad \text{and} \quad V'(\Omega)(\theta) = \int_{\partial\Omega} \theta(x) \cdot n(x)\, ds.$$

Similarly, Lemma 3.4 is useful in order to compute the shape derivative of a perimeter constraint $P(\Omega) = C$. Indeed, we have

$$P(\Omega) = \int_{\partial\Omega} ds \quad \text{and} \quad P'(\Omega)(\theta) = \int_{\partial\Omega} \theta(x) \cdot n(x) H\, ds.$$

Theorem 3.6. *Let Ω be a smooth bounded open set and $\theta \in W^{1,\infty}(\mathbb{R}^d;\mathbb{R}^d)$. Assume that the data f and g as well as the solution u of (2) are smooth, say $f \in H^1(\Omega)^d$, $g \in H^2(\Omega)^d$, $u \in H^2(\Omega)^d$. The shape derivative of (3) is*

$$\begin{aligned} J_1'(\Omega)(\theta) = & \int_{\Gamma_N} \left(2\left[\frac{\partial(g\cdot u)}{\partial n} + Hg\cdot u + f\cdot u\right] - Ae(u)\cdot e(u)\right)\theta\cdot n\, ds \\ & + \int_{\Gamma_D} Ae(u)\cdot e(u)\,\theta\cdot n\, ds. \end{aligned} \tag{8}$$

The shape derivative of (4) is

$$\begin{aligned} J_2'(\Omega)(\theta) = & \int_{\Gamma_N} \left(\frac{C_0}{\alpha} k|u-u_0|^\alpha + Ae(p)\cdot e(u) - f\cdot p \right. \\ & \qquad \left. - \frac{\partial(g\cdot p)}{\partial n} - Hg\cdot p\right)\theta\cdot n\, ds \\ & + \int_{\Gamma_D} \left(\frac{C_0}{\alpha} k|u-u_0|^\alpha - Ae(u)\cdot e(p)\right)\theta\cdot n\, ds. \end{aligned} \tag{9}$$

where p is the adjoint state, assumed to be smooth, i.e. $p \in H^2(\Omega)^d$, defined as the solution of

$$\left\{ \begin{array}{rcll} -\mathrm{div}\,(A\,e(p)) & = & -C_0 k(x)|u-u_0|^{\alpha-2}(u-u_0) & \text{in } \Omega \\ p & = & 0 & \text{on } \Gamma_D \\ \big(Ae(p)\big)n & = & 0 & \text{on } \Gamma_N, \end{array} \right. \tag{10}$$

where C_0 is a constant given by

$$C_0 = \left(\int_\Omega k(x)|u(x)-u_0(x)|^\alpha dx \right)^{1/\alpha - 1}.$$

Remark 3.7. *Remark that there is no adjoint state involved in (8). Indeed the minimization of (3) is a self-adjoint problem which turns out to be easier to solve than (4).*

Proof. Although Theorem 3.6 is a classical result (see e.g. [22], [25], [29], [31]) we briefly sketch its proof for the sake of completeness. To simplify we give

a short, albeit formal, proof due to Céa [15]. We consider a general objective function

$$J(\Omega) = \int_\Omega j\big(x, u(x)\big)\, dx + \int_{\partial\Omega} l\big(x, u(x)\big)\, ds,$$

for which we introduce the Lagrangian defined for $(v, q) \in \big(H^1(\mathbb{R}^d; \mathbb{R}^d)\big)^2$ by

$$\begin{aligned} \mathcal{L}(\Omega, v, q) = \quad & \int_\Omega j(v)\, dx + \int_{\partial\Omega} l(v)\, ds + \int_\Omega Ae(v) \cdot e(q)\, dx - \int_\Omega q \cdot f\, dx \\ & - \int_{\Gamma_N} q \cdot g\, ds - \int_{\Gamma_D} \Big(q \cdot Ae(v)n + v \cdot Ae(q)n \Big) ds. \end{aligned} \tag{11}$$

In (11) q is a Lagrange multiplier for the state equation and its boundary conditions. It is worth noticing that v and q belong to a functional space that does not depend on Ω, so we can apply the usual differentiation rule to the Lagrangian $\mathcal{L}$. The stationarity of the Lagrangian is going to give the optimality conditions of the minimization problem. For a given Ω, we denote by (u, p) such a stationary point. The partial derivative of $\mathcal{L}$ with respect to q, in the direction $\phi \in H^1(\mathbb{R}^d; \mathbb{R}^d)$, after integration by parts leads to

$$\begin{aligned} \langle \frac{\partial \mathcal{L}}{\partial q}(\Omega, u, p), \phi \rangle = 0 = \quad & - \int_\Omega \phi \cdot \Big(\operatorname{div}(Ae(u)) + f \Big) dx \\ & + \int_{\Gamma_N} \phi \cdot \big(\big(Ae(u)\big)n - g \big)\, ds \\ & - \int_{\Gamma_D} u \cdot Ae(\phi)n\, ds. \end{aligned} \tag{12}$$

Taking first ϕ with compact support in Ω gives the state equation. Then, varying the trace function ϕ on Γ_N gives the Neumann boundary condition for u, while varying the corresponding normal stress $\big(Ae(\phi)\big)n$ on Γ_D gives the Dirichlet boundary condition for u. On the other hand, in order to find the adjoint equation, we differentiate $\mathcal{L}$ with respect to v in the direction $\phi \in H^1(\mathbb{R}^d; \mathbb{R}^d)$. This yields

$$\begin{aligned} \langle \frac{\partial \mathcal{L}}{\partial v}(\Omega, u, p), \phi \rangle = 0 \quad = & \int_\Omega j'(u) \cdot \phi\, dx + \int_{\partial\Omega} l'(u) \cdot \phi\, ds \\ & + \int_\Omega Ae(\phi) \cdot e(p)\, dx \\ & - \int_{\Gamma_D} \Big(p \cdot Ae(\phi)n + \phi \cdot Ae(p)n \Big)\, ds. \end{aligned}$$

Integrating by parts we obtain

$$\begin{aligned} \langle \frac{\partial \mathcal{L}}{\partial v}(\Omega, u, p), \phi \rangle = \quad & \int_\Omega \Big(j'(u) - \operatorname{div}(Ae(p)) \Big) \cdot \phi\, dx + \int_{\Gamma_N} \phi \cdot \big(Ae(p)n + l'(u) \big)\, ds \\ & + \int_{\Gamma_D} \Big(\phi \cdot l'(u) - p \cdot Ae(\phi)n \Big) ds. \end{aligned}$$

Taking first ϕ with compact support in Ω gives the adjoint state equation

$$-\mathrm{div}(Ae(p)) = -j'(u) \quad \text{in} \quad \Omega.$$

Then, varying the trace of ϕ on Γ_N yields the Neumann boundary condition

$$\big(Ae(p)\big)n = -l'(u) \quad \text{on} \quad \Gamma_N.$$

Finally, varying the normal stress $\big(Ae(\phi)\big)n$ on Γ_D gives

$$p = 0 \quad \text{on} \quad \Gamma_D.$$

We have therefore found a well-posed boundary value problem for the adjoint state p.

The shape derivative of the objective function is obtained by differentiating

$$J(\Omega) = \mathcal{L}(\Omega, u(\Omega), p(\Omega)),$$

which, by the chain rule theorem, reduces to the partial derivative of $\mathcal{L}$ with respect to Ω in the direction θ

$$J'(\Omega)(\theta) = \frac{\partial \mathcal{L}}{\partial \Omega}(\Omega, u, p)(\theta).$$

Applying Lemma 3.3 and 3.4 we obtain

$$\begin{aligned}
\frac{\partial \mathcal{L}}{\partial \Omega}(\Omega, u, p)(\theta) = \quad & \int_{\partial\Omega} \theta \cdot n \Big(j(u) + Ae(u) \cdot e(p) - p \cdot f \Big) ds \\
& + \int_{\partial\Omega} \theta \cdot n \left(\frac{\partial l(u)}{\partial n} + H\, l(u) \right) ds \\
& - \int_{\Gamma_N} \theta \cdot n \left(\frac{\partial (g \cdot p)}{\partial n} + H\, g \cdot p \right) ds \\
& - \int_{\Gamma_D} \theta \cdot n \left(\frac{\partial h}{\partial n} + H h \right) ds,
\end{aligned} \tag{13}$$

with $h = u \cdot Ae(p)n + p \cdot Ae(u)n$. Taking into account the boundary condition $u = p = 0$ on Γ_D which also implies

$$Ae(u) \cdot e(p) = \mu \frac{\partial u}{\partial n} \cdot \frac{\partial p}{\partial n} + (\mu + \lambda) \left(\frac{\partial u}{\partial n} \cdot n \right) \left(\frac{\partial p}{\partial n} \cdot n \right) \quad \text{on } \Gamma_D,$$

we deduce

$$\begin{aligned}
\frac{\partial \mathcal{L}}{\partial \Omega}(\Omega, u, p)(\theta) = \quad & \int_{\Gamma_N} \theta \cdot n \left(j(u) + Ae(u) \cdot e(p) - p \cdot f - \frac{\partial (g \cdot p)}{\partial n} - H\, g \cdot p \right) ds \\
& + \int_{\Gamma_D} \theta \cdot n \Big(j(u) - Ae(u) \cdot e(p) \Big) ds \\
& + \int_{\partial\Omega} \theta \cdot n \left(\frac{\partial l(u)}{\partial n} + H\, l(u) \right) ds.
\end{aligned}$$

This proof is merely a formal computation (in particular it assumes that u and p are differentiable with respect to the shape Ω) but it can be rigorously justified (see the references quoted above). Of course, if the objective function is the compliance, i.e. $j(u) = f \cdot u$, $l(u) = g \cdot u$ on Γ_N and $l(u) = 0$ on Γ_D, we find that $p = -u$ and the problem is self-adjoint. $\square$

We now give a variant of Theorem 3.6 when the surface loading is a pressure load which is oriented in the direction of the normal vector. In other words, we replace equation (2) by

$$\left\{ \begin{array}{rcll} -\mathrm{div}\,(A\,e(u)) & = & f & \text{in } \Omega \\ u & = & 0 & \text{on } \Gamma_D \\ \big(A\,e(u)\big)n & = & p_0 n & \text{on } \Gamma_N, \end{array} \right. \tag{14}$$

where n is the unit normal vector and $p_0(x)$ is a given scalar function in $H^2(D)$.

Corollary 3.8. *Let Ω be a smooth bounded open set and $\theta \in W^{1,\infty}(\mathbb{R}^d;\mathbb{R}^d)$. Assume that the solution u of (14) is smooth, say $u \in H^2(\Omega)^d$. The shape derivative of the compliance,*

$$J_3(\Omega) = \int_\Omega f \cdot u\,dx + \int_{\Gamma_N} p_0\, n \cdot u\,ds,$$

is

$$\begin{aligned} J_3'(\Omega)(\theta) = & \int_{\Gamma_N} \theta \cdot n \Big(2f \cdot u + 2\mathrm{div}(p_0 u) - Ae(u) \cdot e(u) \Big) ds \\ & + \int_{\Gamma_D} Ae(u) \cdot e(u)\; \theta \cdot n\, ds. \end{aligned} \tag{15}$$

Proof. We rewrite the objective function as

$$J_3(\Omega) = \int_\Omega f \cdot u\,dx + \int_\Omega \mathrm{div}(p_0 u)\,dx.$$

The Lagrangian of the problem is defined for $(v,q) \in \big(H^1(\mathbb{R}^d;\mathbb{R}^d)\big)^2$ by

$$\begin{aligned} \mathcal{L}(\Omega,v,q) = & \int_\Omega f \cdot v\,dx + \int_\Omega \mathrm{div}(p_0 v)\,dx + \int_\Omega Ae(v) \cdot e(q)\,dx - \int_\Omega q \cdot f\,dx \\ & - \int_\Omega \mathrm{div}(p_0 q)\,dx - \int_{\Gamma_D} \Big(q \cdot Ae(v)n + v \cdot Ae(q)n \Big) ds. \end{aligned} \tag{16}$$

One can check that the adjoint state of the problem is $p = -u$ (self-adjoint problem). A computation similar to that of Theorem 3.6 shows that

$$J_3'(\Omega)(\theta) = \frac{\partial \mathcal{L}}{\partial \Omega}(\Omega, u, -u)(\theta),$$

which yields the desired result (15). $\square$

Remark 3.9. *We can generalize Theorem 3.6 to more general objective functions, including functions of the strain or stress. It is also possible to consider non homogeneous Dirichlet boundary conditions in the state equation. The case of a nonlinear model is discussed in Section 8.*

Remark 3.10. *It is possible to further restrict the class of domains by asking that some parts of the boundary Γ_{fixed} do not move. In such a case, the vector field θ must satisfy the constraint (or boundary condition) $\theta \cdot n = 0$ on Γ_{fixed}.*

We now have all the necessary theoretical ingredients to describe a gradient method for the minimization of an objective function $J(\Omega)$. As we have just seen, the general form of its shape derivative is

$$J'(\Omega)(\theta) = \int_{\partial\Omega} v\,\theta \cdot n\,ds,$$

where the function v is given by a result like Theorem 3.6. Ignoring smoothness issues, a descent direction is found by defining a vector field

$$\theta = -v\,n, \tag{17}$$

and then we update the shape Ω as

$$\Omega_t = (\mathrm{Id} + t\theta)\Omega,$$

where $t > 0$ is a small descent step. Formally, we obtain

$$J(\Omega_t) = J(\Omega) - t\int_{\partial\Omega} v^2\,ds + \mathcal{O}(t^2)$$

which guarantees the decrease of the objective function.

There are other possible choices for the definition of the descent direction. Let us first remark that, from a mathematical point of view, formula (17) makes sense only if the resulting vector field θ belongs to $W^{1,\infty}(\mathbb{R}^d, \mathbb{R}^d)$. In view of typical definitions of v, (8) or (9), this is the case only if the state u and adjoint state p, as well as the boundary of Ω, are smooth enough. It is not clear that the optimal shapes, if they exist, are smooth. (However, a recent result of Chambolle and Larsen [14] proves that, in two space dimensions and for a scalar problem, the optimal shape under a perimeter constraint has indeed C^∞ regularity).

If either v or the normal n is not smooth, then it may be desirable to smooth the velocity field vn (this is a classical issue in shape optimization ; see e.g. Chapter 5 in [21]). The main idea is to change the scalar product with respect to which we evaluate a descent direction. For example, working with the H_0^1 scalar product instead of the L^2 one, we need to solve

$$\left\{\begin{array}{rcll} -\Delta\theta & = & 0 & \text{in } \Omega \\ \dfrac{\partial\theta}{\partial n} & = & -v\,n & \text{on } \partial\Omega. \end{array}\right.$$

In other words, we apply the Neumann-to-Dirichlet map to $-v\,n$ which has the effect of increasing of one order the regularity of θ on Γ (with respect to that of $-v\,n$). Integrating by parts, we find

$$\int_\Omega |\nabla\theta|^2 dx = -\int_{\partial\Omega} v\,\theta\cdot n\,ds$$

which shows that θ is a descent direction which guarantees again the decrease of J.

Remark 3.11. *Another possibility is to use the Laplace-Beltrami operator Δ_S on $\partial\Omega$. We first compute a regularization $\tilde{v} = (-\Delta_S)^{-1}v$ and then take the descent direction $\theta\cdot n = -\tilde{v}$. By integration by parts, we find*

$$J'(\Omega)(\theta) = -\int_{\partial\Omega} |\nabla_S\tilde{v}|^2 ds,$$

which clearly shows that θ is a smoother descent direction.

4 Shape parametrization by the level-set method

As described above, the method of shape sensitivity can be (and has been) implemented in a Lagrangian framework. It suffices to mesh Ω and to advect the mesh according to the descent direction θ. However, this implementation suffers at least from two drawbacks. First, if the shape is deformed too much, then it is necessary to remesh which can be very costly (especially in 3-d). Second, different parts of the boundary of the shape may want to merge or split, but as is well known topology changes are very difficult to handle with such Lagrangian or front-tracking methods. Therefore, we favor an Eulerian approach and, following [23] and [27], we use a level-set method to capture the shape Ω on a fixed mesh.

Let a bounded domain $D \subset \mathbb{R}^d$ be the working domain in which all admissible shapes Ω are included, i.e. $\Omega \subset D$. In numerical practice, the domain D will be uniformly meshed once and for all. We parametrize the boundary of Ω by means of a level-set function, following the idea of Osher and Sethian [24]. We define this level-set function ψ in D such that

$$\begin{cases} \psi(x) = 0 & \Leftrightarrow x \in \partial\Omega \cap D, \\ \psi(x) < 0 & \Leftrightarrow x \in \Omega, \\ \psi(x) > 0 & \Leftrightarrow x \in \left(D \setminus \overline{\Omega}\right). \end{cases}$$

The normal n to the shape Ω is recovered as $\nabla\psi/|\nabla\psi|$ and the curvature H is given by the divergence of the normal div$n$ (these quantities are evaluated by finite differences since our mesh is uniformly rectangular). Remark that, although n and H are theoretically defined only on $\partial\Omega$, the level-set method allows to define easily their extension in the whole domain D (this will be useful in the sequel).

The elasticity equations for the state u (as well as the adjoint state p) are extended to the whole domain D by using the so-called "ersatz material" approach. It amounts to fill the holes $D \setminus \Omega$ by a weak phase mimicking void but avoiding the singularity of the rigidity matrix. This is a well-known procedure in topology optimization which can be rigorously justified in some cases [1]. Remark that our method is simpler than the immersed interface method proposed in [27]. More precisely, we define an elasticity tensor $A^*(x)$ which is a mixture of A in Ω and of the weak material mimicking holes in $D \setminus \Omega$

$$A^*(x) = \rho(x)A \quad \text{with} \quad \rho = \begin{cases} 1 & \text{in } \Omega, \\ 10^{-3} & \text{in } D \setminus \Omega. \end{cases} \tag{18}$$

In numerical practice, ρ is piecewise constant in each cell and is adequately interpolated in those cells cut by the zero level-set $\psi = 0$ (the shape boundary). Note that, on the contrary of the homogenization method (or any other generalized material method), the "material density" ρ in (18) is almost always equal to its extreme values (1 or 10^{-3}) and the zone around the shape boundary where it takes intermediate values does not increase in size during the optimization process.

To be more specific, let us consider a simple example for which there is no body force, $f = 0$, and the boundary ∂D of the working domain is decomposed in three parts

$$\partial D = \partial D_D \cup \partial D_N \cup \partial D_0,$$

such that ∂D_D corresponds to Dirichlet boundary conditions, ∂D_N to non-homogeneous Neumann boundary conditions (surface loads $g \neq 0$), and ∂D_0 to homogeneous Neumann boundary conditions (traction-free) respectively. Recall the decomposition (1) of the shape boundary, $\partial\Omega = \Gamma_D \cup \Gamma_N$. Admissible shapes Ω are further constrained to satisfy

$$\Gamma_D \subset \partial D_D, \quad \Gamma_N = \partial D_N \cup \Gamma_0, \tag{19}$$

where Γ_0 supports an homogeneous Neumann boundary conditions (traction-free). In other words, the surface loads g are applied only on a fixed subset of the boundary Γ_N, while the boundary Γ_D, with zero displacement, must be a subset of the fixed boundary ∂D_D. Consequently, the only optimized part of the shape boundary is Γ_0 which is traction free. These conditions are precisely those assumed in all numerical examples of Section 6. Then, the displacement u is computed as the solution of

$$\begin{cases} -\mathrm{div}\,(A^*\, e(u)) &= 0 & \text{in } D \\ u &= 0 & \text{on } \partial D_D \\ \big(A^* e(u)\big)n &= g & \text{on } \partial D_N \\ \big(A^* e(u)\big)n &= 0 & \text{on } \partial D_0. \end{cases} \tag{20}$$

A similar boundary value problem holds for the adjoint p. The homogeneous Neumann boundary condition on Γ_0 is automatically taken into account in the weak formulation of (20), at least in the limit when the ersatz material goes to

zero. The case of body forces and surface loads on the optimized boundary is treated in Section 7.

Following the optimization process, the shape is going to evolve according to a fictitious time which corresponds to descent stepping (we shall come back to this issue in the next section). As is well-known, if the shape is evolving in time, then the evolution of the level-set function is governed by a simple Hamilton-Jacobi equation. To be precise, assume that the shape $\Omega(t)$ evolves in time $t \in \mathbb{R}^+$ with a normal velocity $V(t,x)$. Then

$$\psi\Big(t, x(t)\Big) = 0 \quad \text{for any } x(t) \in \partial\Omega(t).$$

Differentiating in t yields

$$\frac{\partial \psi}{\partial t} + \dot{x}(t) \cdot \nabla\psi = \frac{\partial \psi}{\partial t} + V n \cdot \nabla\psi = 0.$$

Since $n = \nabla\psi/|\nabla\psi|$ we obtain

$$\frac{\partial \psi}{\partial t} + V|\nabla\psi| = 0.$$

This Hamilton-Jacobi equation is posed in the whole box D, and not only on the boundary $\partial\Omega$, if the velocity V is known everywhere (as will be the case in the sequel).

5 Optimization algorithm

For the minimization problem

$$\inf_{\Omega \in \mathcal{U}_{ad}} J(\Omega),$$

we computed a shape derivative

$$J'(\Omega)(\theta) = \int_{\partial\Omega} v\, \theta \cdot n \, ds,$$

where the function $v(u,p,n,H)$ is given by a result like Theorem 3.6. Remark that, since n and H, as well as the state u and the adjoint state p, are computed everywhere in D, the integrand v in the shape derivative is defined throughout the domain D and not only on the free boundary $\partial\Omega$. Therefore, we can define a descent direction in the whole domain D by

$$\theta = -v\, n.$$

(It is also possible to regularize θ but that does not change the sequel). The normal component $\theta \cdot n = -v$ is therefore the advection velocity in the Hamilton-Jacobi equation

$$\frac{\partial \psi}{\partial t} - v|\nabla\psi| = 0. \tag{21}$$

Transporting ψ by (21) is equivalent to move the boundary of Ω (the zero level-set of ψ) along the descent gradient direction $-J'(\Omega)$. Our proposed algorithm is an iterative method, structured as follows:

1. Initialization of the level-set function ψ_0 corresponding to an initial guess Ω_0.
2. Iteration until convergence, for $k \geq 0$:
   (a) Computation of the state u_k and adjoint state p_k through two problems of linear elasticity posed in Ω_k, approximated by (20).
   (b) Deformation of the shape by solving the transport Hamilton-Jacobi equation (21). The new shape Ω_{k+1} is characterized by the level-set function ψ_{k+1} solution of (21) after a time step Δt_k starting from the initial condition $\psi_k(x)$ with velocity $-v_k$ computed in terms of u_k and p_k. The time step Δt_k is chosen such that $J(\Omega_{k+1}) \leq J(\Omega_k)$.
3. From time to time, for stability reasons, we also reinitialize the level-set function ψ by solving (22).

The Hamilton-Jacobi equation (21) is solved by an explicit first order upwind scheme (see e.g. [26]) on a Cartesian grid. In one space dimension, the scheme reads

$$\frac{\psi_i^{n+1} - \psi_i^n}{\Delta t} + \min(V_i^n, 0)\, g^-(D_x^+\psi_i^n, D_x^-\psi_i^n) + \max(V_i^n, 0)\, g^+(D_x^+\psi_i^n, D_x^-\psi_i^n) = 0$$

with $D_x^+\psi_i^n = \dfrac{\psi_{i+1}^n - \psi_i^n}{\Delta x}$, $D_x^-\psi_i^n = \dfrac{\psi_i^n - \psi_{i-1}^n}{\Delta x}$, and

$$g^+(d^+, d^-) = \sqrt{\min(d^+, 0)^2 + \max(d^-, 0)^2},$$

$$g^-(d^+, d^-) = \sqrt{\max(d^+, 0)^2 + \min(d^-, 0)^2}.$$

We also implemented a second order scheme in order to improve accuracy (see Figure 12 for some comparisons). The boundary conditions for ψ are of Neumann type. Since this scheme is explicit in time, its time stepping must satisfy a CFL condition. Remark that the time step issued from this CFL condition is usually much smaller than the time step Δt_k which plays the role of the descent step in the minimization of $J(\Omega)$. Remark also that one explicit time step for (21) is much cheaper, in terms of CPU time and memory requirement, than the solution of the state equation (2) or adjoint state equation (10). Therefore, for each iteration k in the above algorithm (corresponding to a single evaluation of u_k and p_k), we perform several explicit time steps of the Hamilton-Jacobi equation (21). The number of such time steps per iteration k is monitored by the decrease of $J(\Omega_k)$.

In practice, our algorithm never creates new holes or boundaries in 2-d if the Hamilton-Jacobi equation (21) is solved under a strict CFL condition because

it satisfies a maximum principle (there is no nucleation mechanism for new holes). However the level-set method is well known to handle easily topology changes, i.e. merging or cancellation of holes. Therefore, our algorithm is able to perform topology optimization. In 2-d, the best results are obtained if the number of holes of the initial design is sufficiently large (see Figure 1). The situation is different in 3-d where new holes easily appear by pinching a thin wall (see Figure 25), and then the initial topology is less important.

Remark 5.1. *One of the main advantage of the level-set method is that we never have to know where precisely is the boundary $\partial\Omega$. In particular, the same numerical scheme for solving the Hamilton-Jacobi equation (21) is applied everywhere in the working domain D. Another advantage of the level-set method comes from the simple formula to compute the normal n and the mean curvature $H = \mathrm{div} n$ (which plays an important role in perimeter penalization).*

In order to regularize the level-set function (which may become too flat or too steep), we reinitialize it periodically by solving

$$\left\{ \begin{array}{rcll} \dfrac{\partial \psi}{\partial t} + \mathrm{sign}(\psi_0)\Big(|\nabla \psi| - 1\Big) & = & 0 & \text{in } D \times \mathbb{R}^+, \\ \psi(t=0,x) & = & \psi_0(x) & \text{in } D, \end{array} \right. \tag{22}$$

which admits as a stationary solution the signed distance to the initial interface $\{\psi_0(x) = 0\}$ (see for example Figure 7). In numerical practice, reinitialization is very important because the level-set function often becomes too steep which implies a bad approximation of the normal n or of the curvature H.

6 Numerical examples

In all computations we use a quadrangular mesh for both the level-set function and the elastic displacement. We use $Q1$ finite elements for the elasticity analysis. All test cases have the following data, unless otherwise specified. The Young modulus E of material A is normalized to 1 and the Poisson ratio ν is fixed to 0.3. The void or holes are mimicked by an ersatz material with the same Poisson ratio and Young modulus 10^{-3}. For each elasticity analysis (that we shall call iteration in the sequel) we perform 20 explicit time steps of the first-order scheme for the Hamilton-Jacobi transport equation. This number is automatically reduced if the objective function is not decreasing. We also reinitialize the level-set function every 5 time steps of transport by performing 5 explicit time steps of equation (22).

6.1 2-d cantilever

In the two-dimensional setting $d = 2$ we first study a medium cantilever problem. The working domain is a rectangle of size 2×1 discretized with a rectangular 80×40 mesh, with zero displacement boundary condition on the left side and a

unit vertical point load at the middle of the right side (see Figure 1). Admissible shapes must satisfy the constraint (19), i.e.

$$\partial\Omega = \Gamma_D \cup \partial D_N \cup \Gamma_0,$$

where the shape Dirichlet boundary Γ_D is a subset of the fixed boundary ∂D_D, the surface loads g are applied only the fixed boundary ∂D_N, and Γ_0, which is traction free, is varying during the optimization process. There are no body forces, i.e. $f \equiv 0$ in (2). The objective function is a combination of the compliance and of the weight of the structure

$$J(\Omega) = \int_{\partial D_N} g \cdot u \, ds + \ell \int_\Omega dx, \tag{23}$$

where $\ell = 100$ is a fixed Lagrange multiplier for the weight constraint, and $g = 0$ on Γ_0. The boundary conditions and two initial configurations with different number of holes are displayed on Figure 1. Under these assumptions, the shape derivative of (23) is a special case of Theorem 3.6, namely

$$J'(\Omega)(\theta) = \int_{\Gamma_0} \Big(\ell - Ae(u) \cdot e(u)\Big)\theta \cdot n \, ds, \tag{24}$$

since $\theta \cdot n = 0$ on Γ_D and on ∂D_N where $g \neq 0$.

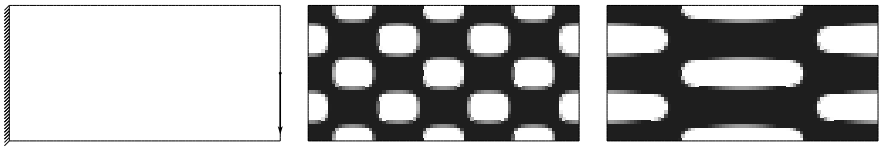

Figure 1: Boundary conditions and two initializations of a 2-d cantilever

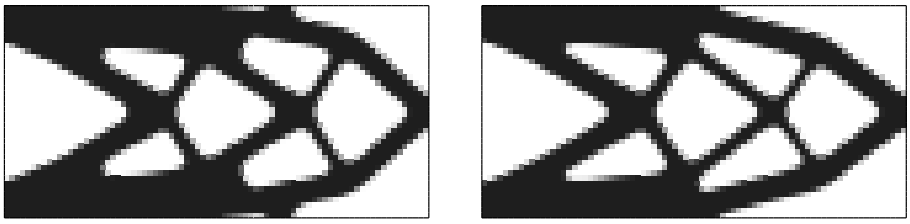

Figure 2: Iterations 10 and 50 of the two-dimensional cantilever initialized as in Figure 1 (middle)

The algorithm converges smoothly to a (local) minimum which strongly depends, of course, on the initial topology as can be checked on Figures 2 and 3, displaying the optimal shapes as well as an intermediate result. We run 50 iterations in order to show the good convergence and stability properties of our

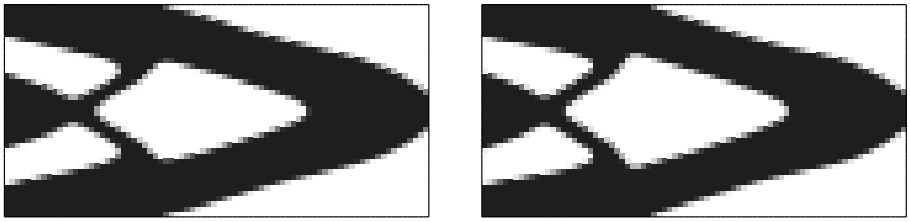

Figure 3: Iterations 10 and 50 of the two-dimensional cantilever initialized as in Figure 1 (right)

algorithm, but it is clear that it has converged in a much smaller number of iterations (see Figure 4). One can also check on Figure 5 that the L^2 norm of the gradient of the objective function is decreasing, although it does not converge to zero, due to numerical approximations. Our algorithm is just a steepest descent gradient method; of course, its convergence can be speed up by using, for example, a quasi-Newton algorithm.

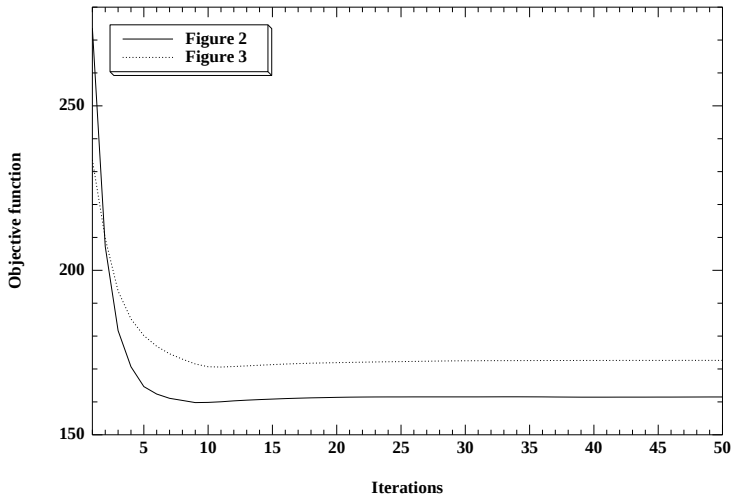

Figure 4: Convergence of the objective function for the two-dimensional cantilever of Figures 2 and 3

For a given initial guess our results are mesh-independent. For example, we performed the same cantilever problem on a finer 160×80 mesh. Since we did not change any other parameters and because of the CFL condition for the Hamilton-Jacobi transport equation, the time step is two times smaller and we need to run 100 iterations instead of 50. One can check that the final shape in Figure 6 is almost identical to the final one in Figure 2.

The effect of reinitialization is best seen on fine meshes and is less important on coarse meshes. For the previous cantilever example on a 160×80 mesh, we

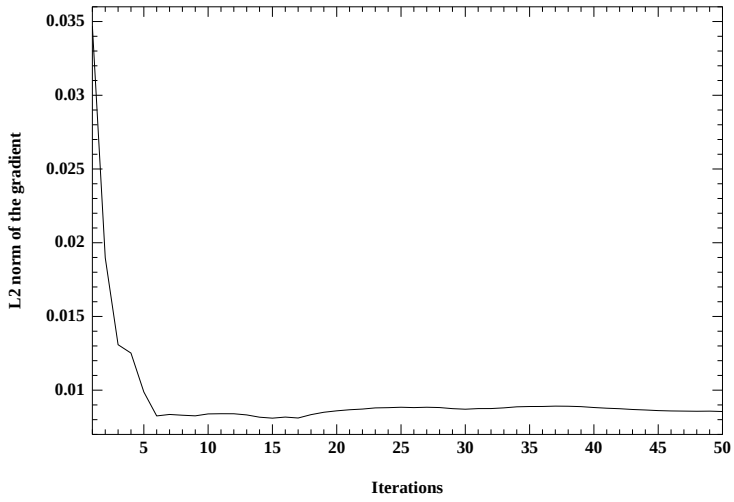

Figure 5: Convergence of the L^2 norm of the gradient of the objective function for the two-dimensional cantilever of Figure 2

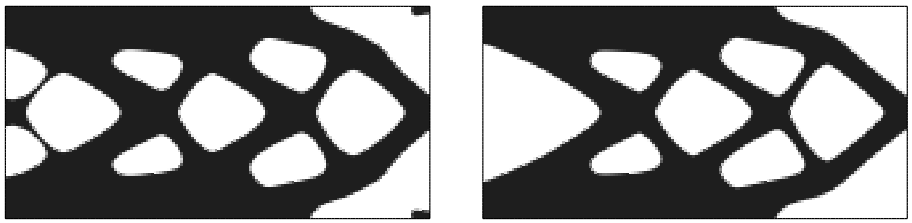

Figure 6: Iterations 50 and 100 of the two-dimensional cantilever on a finer 160×80 mesh initialized as in Figure 1 (middle)

can see on Figure 8 that no reinitialization yields a poorer convergence than reinitializing every 5 time steps of transport (i.e. 4 times every elasticity iteration). Remark on Figure 7 the effect of reinitialization on the final level-set function ψ. On the other hand, Figure 8 shows that there is no clear difference on the objective function between a first-order or second-order scheme for the Hamilton-Jacobi equations (both the transport equation (21) and the reinitialization equation (22)). However, second-order accuracy improves greatly the efficiency of the reinitialization process (it is less important on the transport equation). The optimal shapes for first or second order schemes are slightly different, mainly near the boundary of the working domain D (compare Figures 6 and 11).

As is well known, a necessary condition of optimality for a shape minimizing the objective function (23) is that the "velocity" $\Big(\ell - Ae(u) \cdot e(u)\Big)$ is zero on the boundary. Figure 9 displays the isocontours of this scalar velocity. One can

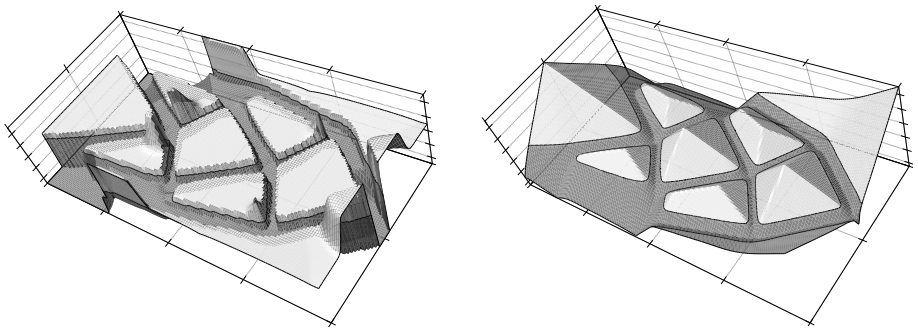

Figure 7: Level-set function for the 2-d cantilever without reinitialization (left) and with reinitialization (right)

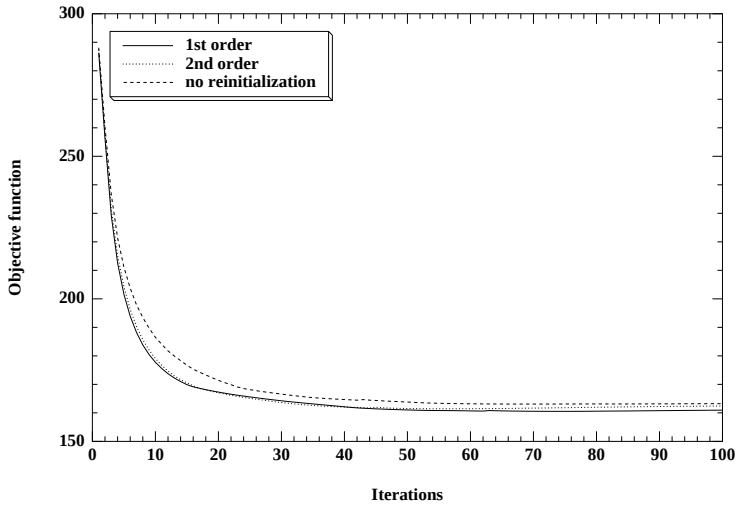

Figure 8: Convergence of the objective function for the two-dimensional cantilever of Figure 6 with various options

check that the velocity is approximately zero on the boundary.

6.2 Comparison with the homogenization method

We compare the level-set method with the homogenization method as described in [1], [2]. For "good" initializations, the numerical result of our level-set method are similar to those obtained by the homogenization method (see Chapter 5 in [1]). To make a precise comparison we study the medium cantilever, as in the previous subsection, with a fine mesh (160×80). The Lagrange multiplier is now fixed to the value $\ell = 150$ and we use a second order scheme. Figure 10 shows the optimal cantilever obtained by the homogenization method, while

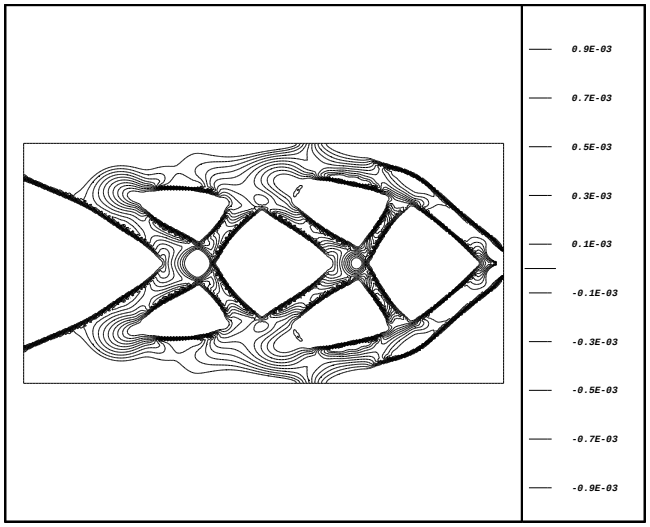

Figure 9: Scalar velocity $\Big(\ell - Ae(u) \cdot e(u)\Big)$ for the 2-d cantilever of Figure 6

Figure 11 displays two results of the level-set method corresponding to two different initializations. The shapes are slightly different but the best result is obtained by homogenization as can be checked on Figure 12. Remark that the bump on the homogenization convergence curve in Figure 12 is due to the penalization process, while the small bump in the convergence curve of the level-set method for initialization 2 is due to a change of topology (bar elimination).

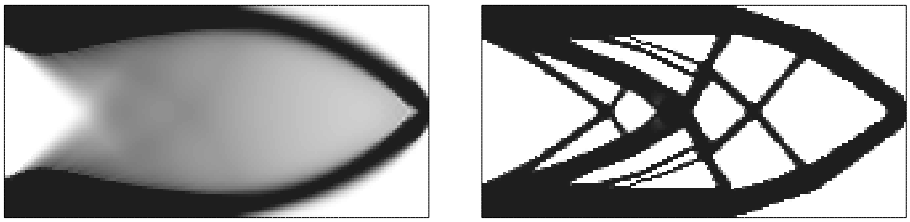

Figure 10: Cantilever computed with the homogenization method. Composite (left) and penalized solution (right)

6.3 2-d bridge

The next example in dimension $d = 2$ is a bridge problem. The working domain is a rectangle of size 2×1.2 discretized with a rectangular 80×48 mesh, at the two lower corners the vertical displacement is zero, and a unit vertical force is applied at the middle of the bottom side (see Figure 13). We again impose that the shape Dirichlet boundary Γ_D is a subset of the fixed boundary ∂D_D, that

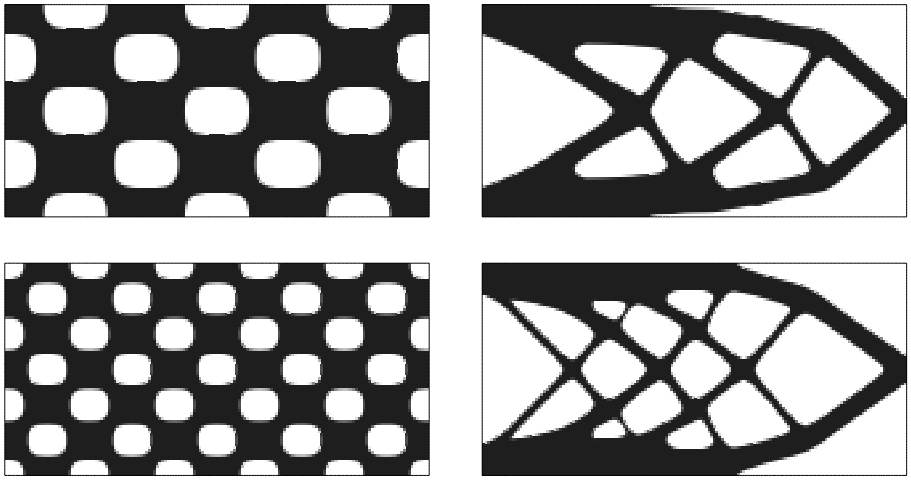

Figure 11: Level-set method: initializations 1 and 2 (left) and resulting optimal designs (right)

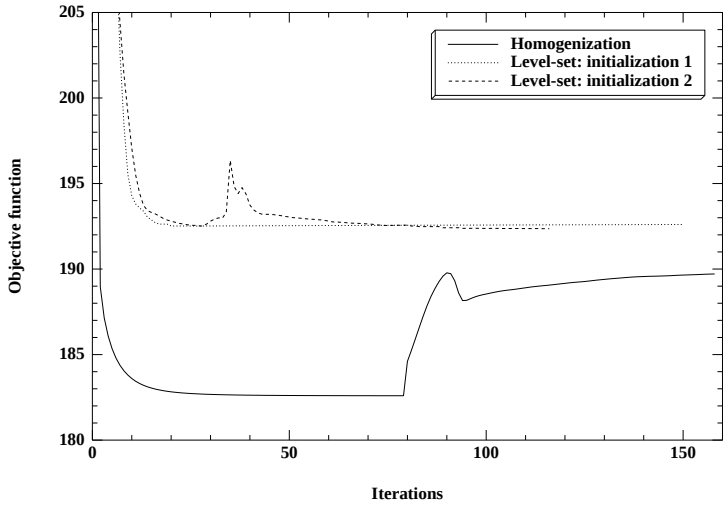

Figure 12: Convergence of the objective function for the two-dimensional cantilevers of Figures 10 and 11

the surface loads g are applied only the fixed boundary ∂D_N, and that only the traction free boundary Γ_0 is varying during the optimization process. We neglect body forces, i.e. $f \equiv 0$. The objective function is (23) and its shape derivative is (24). The Lagrange multiplier for the weight constraint is $\ell = 30$. The optimal design is displayed in Figure 14. We run the same problem with a

perimeter constraint, namely we minimize

$$J(\Omega) = \int_{\partial D_N} g \cdot u \, ds + \ell \int_\Omega dx + \ell' \int_{\partial\Omega} ds, \tag{25}$$

with $\ell' = 1$. Recall that the derivative of the perimeter is the curvature as stated in Remark 3.5. We clearly see on Figure 15 that the resulting optimal shape has fewer holes although the initialization was the same.

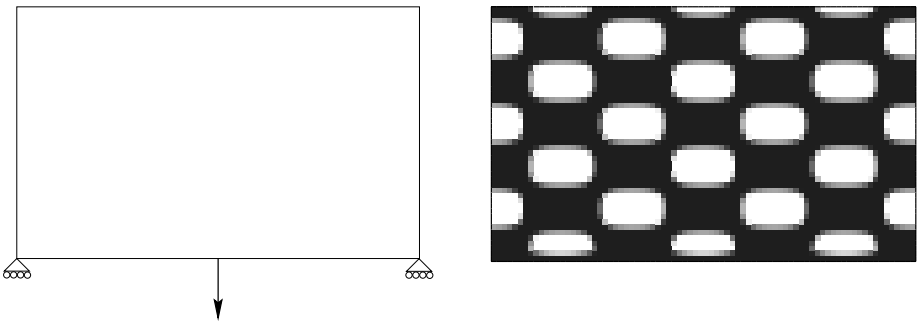

Figure 13: Boundary conditions and initialization of the bridge problem.

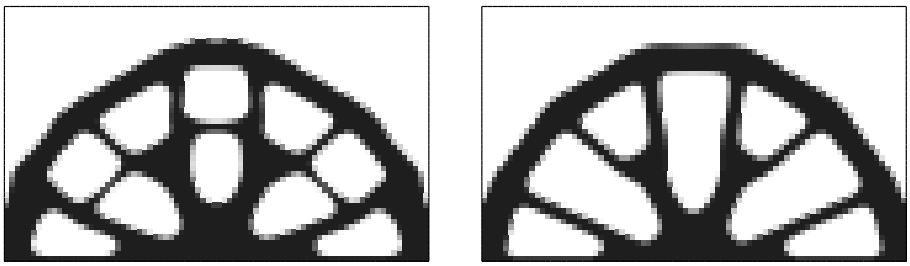

Figure 14: Iterations 30 and 50 of the two-dimensional bridge initialized as in Figure 13

6.4 3-d examples

One advantage of the level-set method is its easy extension to three space dimensions. We therefore turn to a first three-dimensional test case: the 3-d cantilever. The domain is a parallelepiped of dimensions $5 \times 2.4 \times 3$ discretized with $50 \times 24 \times 30$ elements. The right wall is fixed and a unit force is applied downward on the middle of the left wall. Due to symmetry, the computation is performed on half of the domain. We still minimize the weighted sum (23) of the compliance and the weight for a Lagrange multiplier $\ell = 15$. Figure 16 shows the initial and optimal designs.

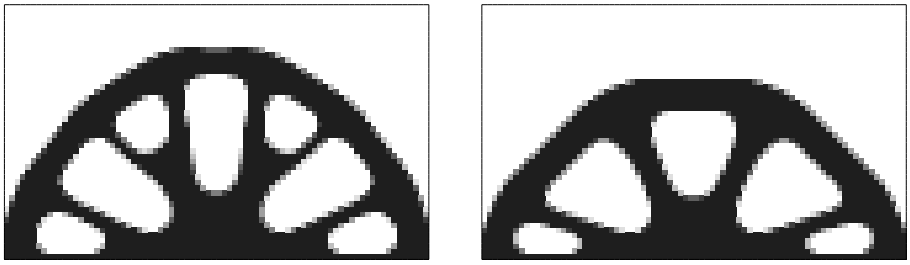

Figure 15: Iterations 50 and 200 of the two-dimensional bridge, initialized as in Figure 13, with a perimeter constraint

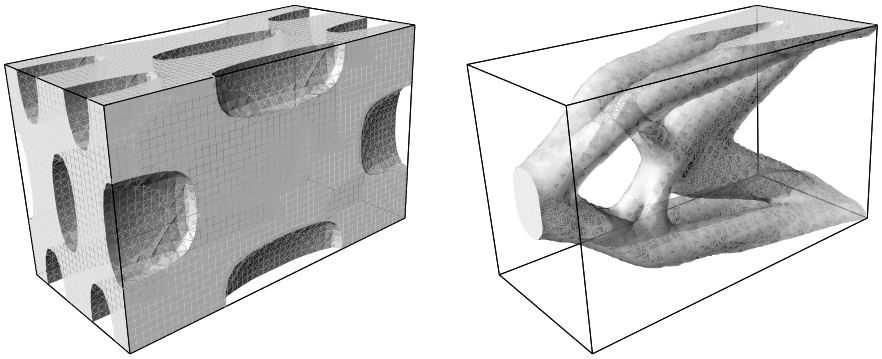

Figure 16: Initial guess and optimal shape for the three-dimensional cantilever.

A second example is that proposed in [2]: the optimal electrical mast. The workspace is a T-like box. Two symmetric vertical loads are applied in the middle of the lower edges of the horizontal part of the T and represent the force exerted by the wires on the mast. Simply supported boundary conditions are imposed at the corners of the base of the T. We still minimize the weighted sum (23) of the compliance and the weight for a Lagrange multiplier $\ell = 2$. Only a quarter of the object is computed, by virtue of the symmetries. The mesh of the T-box is made of a $24 \times 12 \times 28$ bar and a $12 \times 12 \times 48$ foot, for a total number of 14976 hexaedral elements. Starting with an initial design with regularly distributed holes, the resulting optimal shape, displayed on Figure 17, evokes the shape of actual electric masts.

6.5 Another objective function

We now give a numerical example for the minimization of the least square objective function (4). This is a classical gripping mechanism test case which is described, e.g., in [1], [28]. The working domain is a rectangle of size 5×4 with a rectangular hole of size 0.2×1.4 on the middle of the left side. By symmetry, only the upper half of the domain is meshed with a rectangular 50×20 mesh.

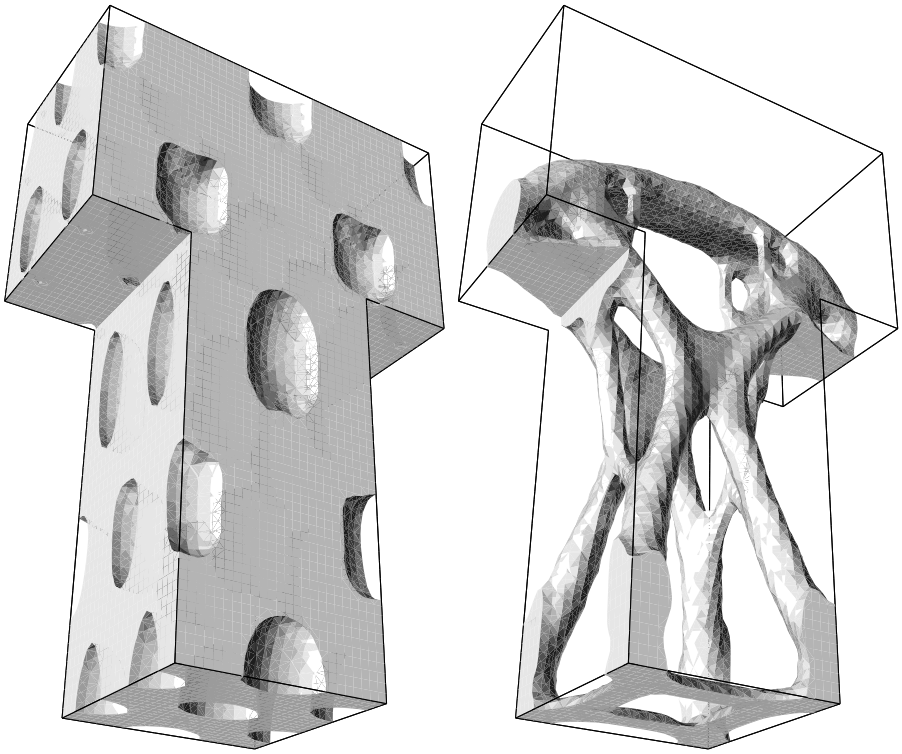

Figure 17: Initial guess and optimal shape for the three-dimensional electrical mast.

In the objective function (4) the localizing factor $k(x)$ is zero except on the black zone on the left side (the jaws of the mechanism) where it is equal to 1, whereas the target displacement $u_0(x)$ is set to $(-100, 0)$ in the upper left black zone (see Figure 18). This objective function has been cooked up in order to obtain a gripping mechanism for which the jaws close. From a mathematical point of view the main difference between this test case and the previous ones is that it needs an adjoint system in order to evaluate the derivative. Figure 19 shows the resulting optimal shape.

We perform the same optimization in 3-d. A uniform pressure load is applied on the left side of the box, while the upper and lower sides are fixed. The initialization and the optimal deformed shape are displayed on Figure 20. One can see in Figure 21 that the algorithm is stable and convergence occurs quite early during the process.

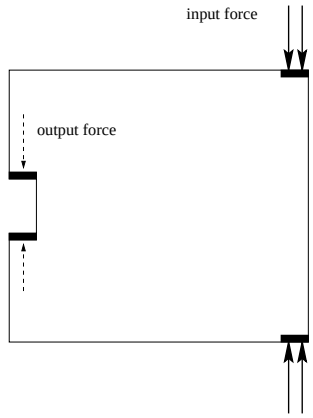

Figure 18: Boundary conditions for a plane gripping mechanism.

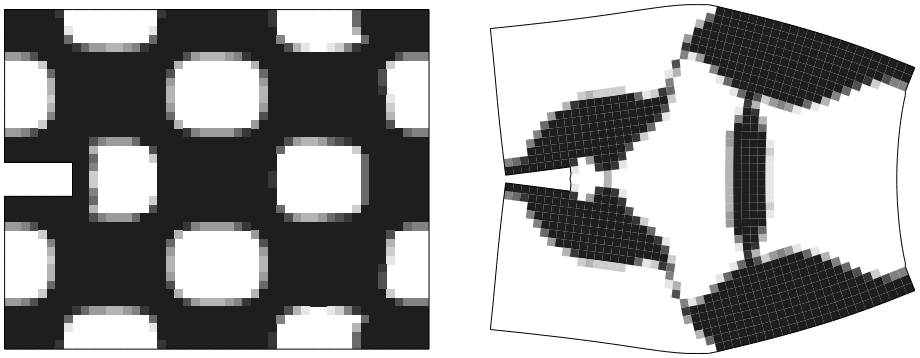

Figure 19: Initialization, and deformed optimal shape of a plane gripping mechanism.

7 Application to design-dependent loads

Until now and in the whole section 6 we neglected the body forces f and the surface loads g were applied on a fixed part of the shape boundary ∂D_N. In such a case the elasticity system was simply (20). We now explain how to generalize it for more complicated loadings, including design-dependent loads as discussed for example in [11].

In the case of body forces f, it suffices to extend them by 0 in $D \setminus \Omega$. This is easily done by multiplying f by the characteristic function χ defined in terms of the level-set function ψ by

$$\chi(x) = \begin{cases} 0 & \text{if } \psi(x) > 0, \\ 1 & \text{if } \psi(x) < 0. \end{cases}$$

Since our code discretizes the body forces as piecewise constants in each cell,

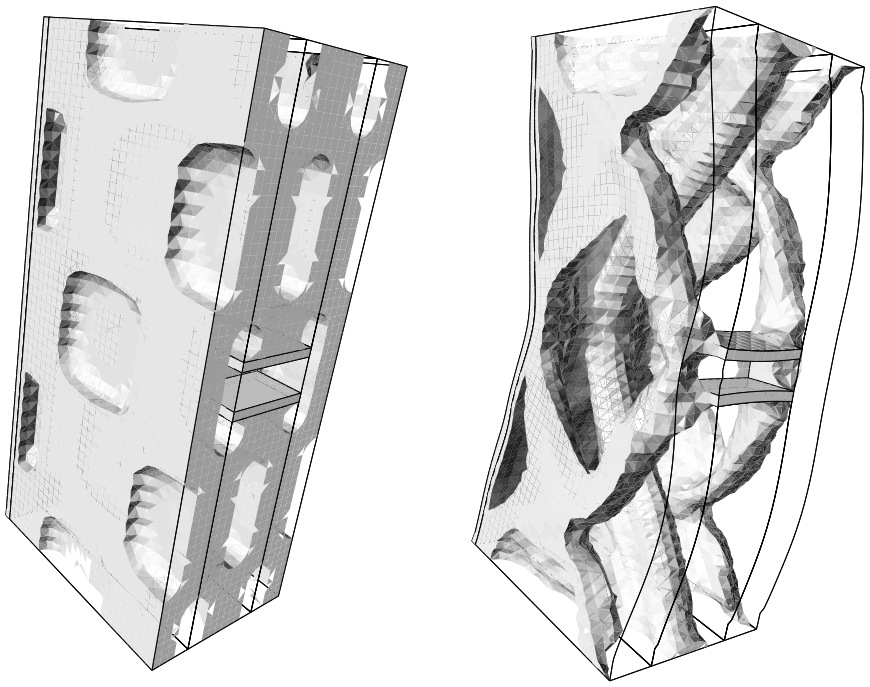

Figure 20: Initialization and deformed optimal configuration of a 3-d gripping mechanism.

the characteristic function χ is also constant in each cell. In the cells cut by the zero level-set we use the same interpolation procedure as that used for the density ρ defined in (18).

Surface loads g which are applied on the moving shape boundary Γ_0 (see (19) for this notation) are called design-dependent since they depend on the position of the shape (recall that g is defined a priori everywhere in D). Numerically, we shall replace these surface loads by equivalent volume forces using the fact that, in the variational formulation of (2), they appear as

$$\int_{\Gamma_0} g \cdot u \, ds = \int_D \delta_{\Gamma_0} g \cdot u \, dx,$$

where $\delta_{\Gamma_0}(x)$ is the Dirac mass function concentrated on Γ_0. Remark that

$$\nabla(\text{sign}(\psi)) = 2\delta_{\Gamma_0} n, \tag{26}$$

and thus

$$\frac{1}{2}|\nabla(\text{sign}(\psi))| = \delta_{\Gamma_0}.$$

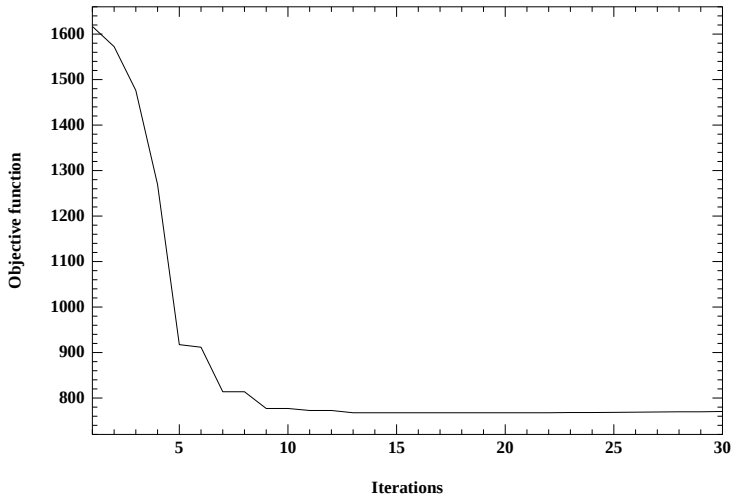

Figure 21: Convergence of the objective function for the three-dimensional gripping mechanism of Figure 20.

Introducing the following approximation of the sign function

$$\mathrm{s}(x) = \frac{\psi(x)}{\sqrt{\psi(x)^2 + \epsilon^2}},$$

where $\epsilon > 0$ is a small parameter chosen to regularize the jump over a few mesh elements. In all our computations, ϵ is equal to $h/20$ where h is the typical element size. This value spreads the jump in the sign function over 2 cells in average. It allows classically to define an approximation $d(x)$ of the Dirac function δ_{Γ_0}

$$d(x) = \frac{1}{2}|\nabla \mathrm{s}(x)|.$$

Finally, recalling definition (18) of the mixture A^* of the true and ersatz materials, the elasticity equations in the working domain D are given by

$$\left\{ \begin{array}{rcll} -\mathrm{div}\,(A^*\, e(u)) & = & \chi\, f + d\, g & \text{in } D \\ u & = & 0 & \text{on } \partial D_D \\ \big(A^* e(u)\big) n & = & g & \text{on } \partial D_N \\ \big(A^* e(u)\big) n & = & 0 & \text{on } \partial D_0. \end{array} \right. \tag{27}$$

As an example we computed the optimal shape of a vertical mast submitted to a uniform horizontal surface load $g = (1, 0, 0)$. This is a reinforcement problem for a column which is not subject to optimization. The objective function is the compliance

$$J(\Omega) = \int_{\Gamma_0} g \cdot u \, ds + \ell \int_{\Omega} dx,$$

with $\ell = 100$. The size of the working domain D is $4 \times 1 \times 4$. The bottom of the box is fixed, i.e. equal to ∂D_D, the other sides are free, i.e. equal to ∂D_0, and $\partial D_N = \emptyset$. In truth we applied g only where its scalar product with the exterior normal n is negative: this is a very crude model of the effect of the wind. The resulting optimal shape can be seen on Figure 22.

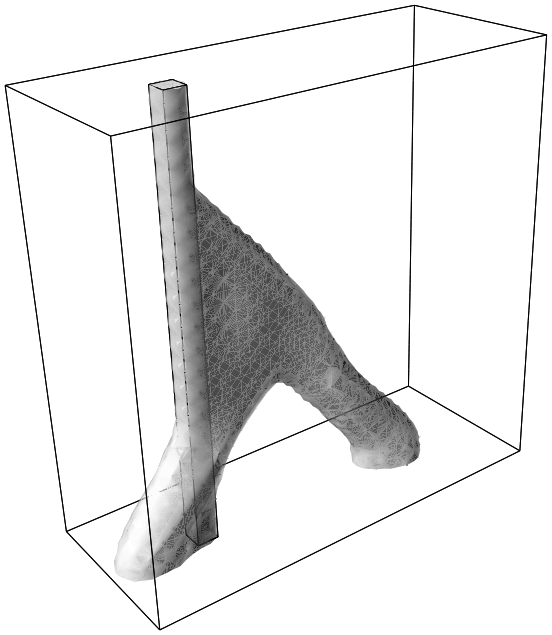

Figure 22: Vertical mast reinforced to support a uniform horizontal load (from the left) modelizing the effects of the wind

Another type of design-dependent loads is the case of a pressure load $p_0\, n$ where p_0 is a given pressure distribution. In other words, we now consider the elasticity system (14). Note that this load depends on the normal to the boundary and therefore, if two different configurations of the free boundary Γ_0 pass through the same point, the loads at this point may be different for each configuration according to the orientation of Γ_0. Once again, the surface loads give the following contribution in the variational formulation

$$\int_{\Gamma_0} p_0\, n \cdot u\, ds = \int_D p_0 \delta_{\Gamma_0} n \cdot u\, dx,$$

and from (26) we define an approximation of the function $(\delta_{\Gamma_0} n)$ by

$$\frac{1}{2} \nabla \mathrm{s}.$$

We therefore replace the surface pressure load by the approximate volume force $\frac{p_0}{2} \nabla \mathrm{s}$ which is zero in the whole domain D except in a neighborhood of Γ_0. One

can see on the 2-d example of Figure 23 that the approximate volume force is really close to a surface pressure load.

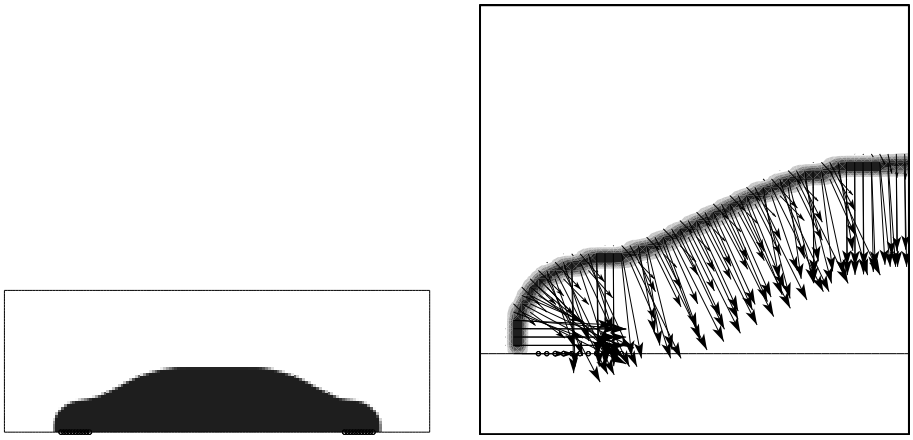

Figure 23: Optimal shape under a uniform pressure load with two anchor points (left). Applied forces on a zoomed area of the same structure (right)

The objective function is again the compliance

$$J(\Omega) = \int_{\Gamma_0} p_0\, n \cdot u\, ds + \ell \int_{\Omega} dx,$$

with $\ell = 100$. Its shape derivative is computed by Corollary 3.8. The size of the working domain D is $4 \times 4 \times 1$. In 3-d we impose 5 fixed (anchor) points on the bottom of the domain and a uniform pressure load $p_0 = -1$ on the free boundary Γ_0. If there is an additional unit vertical load in the middle of the bottom side we obtain a nice starfish as can be seen of Figure 24. Without this vertical load, we obtain a more complex topology as can be checked on Figure 25. Remark that the initialization in both cases was a convex domain and that the level-set algorithm was able to create holes in the case of Figure 25.

8 Generalization to nonlinear elasticity

8.1 Model and shape derivative

In this section we consider a nonlinear hyperelastic model (see [18]). If u is the displacement field, $F = (I + \nabla u)$ denotes the deformation gradient and the boundary value problem writes in the reference configuration Ω (i.e. the undeformed configuration):

$$\left\{ \begin{array}{rcll} -\mathrm{div}\,(T(F)) & = & f & \text{in } \Omega \\ u & = & 0 & \text{on } \Gamma_D \\ T(F)n & = & g & \text{on } \Gamma_N. \end{array} \right. \tag{28}$$

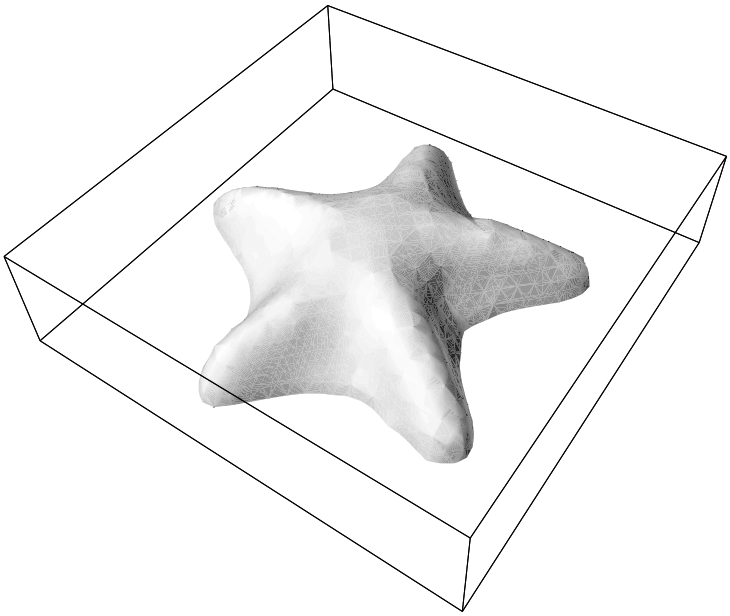

Figure 24: Optimal shape under a uniform pressure load with five anchor points and a vertical force at center.

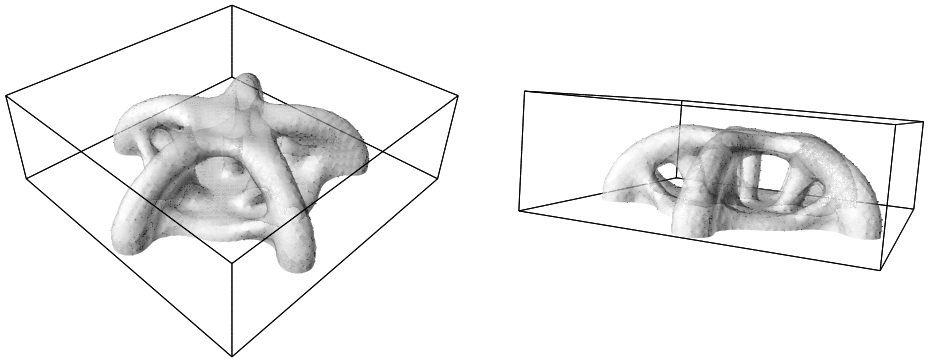

Figure 25: Two views of the optimal shape under a uniform pressure load with five anchor points.

For the sake of simplicity, the volume forces f and the surface loads g are supposed to be dead loads, i.e. independent of the displacement u.

If the material is hyperelastic, the first Piola-Kirchhoff stress tensor T derives from a potential $W(F)$ (supposed smooth enough) called stored energy function

$$T_{ij} = \frac{\partial W(F)}{\partial F_{ij}}, \quad i, j \in \{1, \dots, d\},$$

and for any deformation tensor F, the elasticity tensor $\mathcal{A}(u)$ (which is the tangential operator around F) is defined by

$$\mathcal{A}_{ijkl}(u) = \frac{\partial T_{ij}(F)}{\partial F_{kl}} = \frac{\partial^2 W(F)}{\partial F_{ij} \partial F_{kl}}.$$

The variational formulation of (28) is

$$\int_\Omega T(F) \cdot \nabla v \, dx - \int_\Omega f \cdot v \, dx - \int_{\Gamma_N} g \cdot v \, ds = 0 \quad \forall v \in H^1(\Omega)^d, v = 0 \text{ on } \Gamma_D,$$

and it is formally equivalent to a stationarity condition on the energy

$$I(u) = \int_\Omega W(I + \nabla u) \, dx - \int_\Omega f \cdot u \, dx - \int_{\Gamma_N} g \cdot u \, ds$$

Remark 8.1. *The minimization problem*

$$\min_v I(v)$$

has a solution if W satisfies some convexity, growth and regularity conditions (see [7]) but the question of existence of solutions to the boundary value problem (28) is still open.

We give a variant of Theorem 3.6 for nonlinear elasticity and for the following objective function

$$J(\Omega) = \int_\Omega j\big(x, u(x)\big) \, dx + \int_{\partial\Omega} l\big(x, u(x)\big) \, ds, \tag{29}$$

where j and l are smooth functions satisfying suitable growth conditions (so that $J(\Omega)$, as well as the ajoint problem (30), make sense). In order to avoid unnecessary technical complications, we assume enough smoothness of the data and existence and uniqueness of solutions in simple functional spaces.

Theorem 8.2. *Let Ω be a smooth bounded open set and $\theta \in W^{1,\infty}(\mathbb{R}^d; \mathbb{R}^d)$. Assume that the data f and g are smooth ($f \in H^1(\Omega)^d$, $g \in H^2(\Omega)^d$) and that there exists a unique smooth solution $u \in H^2(\Omega)^d$ of (28). Assume also that there exists a unique smooth solution $p \in H^2(\Omega)^d$ of the following (linear) adjoint problem*

$$\left\{ \begin{array}{rcll} -\operatorname{div}\left(\mathcal{A}(u) \nabla p\right) & = & -j'(u) & \text{in } \Omega \\ p & = & 0 & \text{on } \Gamma_D \\ \big(\mathcal{A}(u) \nabla p\big) n & = & -l'(u) & \text{on } \Gamma_N. \end{array} \right. \tag{30}$$

Assuming that $\mathcal{A}(u)$ and $\mathcal{A}(p)$ are coercive, the shape derivative of (29) is

$$\begin{aligned} J'(\Omega)(\theta) = & \int_{\partial\Omega} \theta \cdot n \Big(j(u) + T(I+\nabla u)\cdot\nabla p - p\cdot f \Big)\, ds \\ & + \int_{\partial\Omega} \theta\cdot n \left(\frac{\partial l(u)}{\partial n} + H\, l(u) \right) ds \\ & - \int_{\Gamma_N} \theta\cdot n \left(\frac{\partial (g\cdot p)}{\partial n} + H\, g\cdot p \right) ds \\ & - \int_{\Gamma_D} \theta\cdot n \left(\frac{\partial h}{\partial n} \right) ds, \end{aligned} \tag{31}$$

where $h = u\cdot T(I+\nabla p)n + p\cdot T(I+\nabla u)n$.

Remark 8.3. *In a nonlinear setting, the compliance is obtained by taking $j(x,u) = f\cdot u$ and $l(x,u) = g\cdot u$ in (29). In such a case, the adjoint state p is different from $(-u)$.*

Remark 8.4. *The adjoint problem (30) is linear. The elasticity tensor $\mathcal{A}(u)$ involved is the tangential operator around the solution u. If the numerical method used to solve the problem (28) is Newton-like, this elasticity tensor has to be computed during the resolution of (28). Furthermore, if the linear systems are solved by a direct solver (Cholesky factorization), then the additional cost of the adjoint problem is very small since the rigidity matrix has already being factorized during the resolution of the direct problem.*

Remark 8.5. *Usually the stored elastic energy $W(F)$ is strongly convex near the identity, so that $\mathcal{A}(u)$ is coercive if u is close to 0 (and thus, automatically, there exists a unique solution p to the adjoint problem). Such a condition is met if, for example, the applied loads f and g are sufficiently small. Furthermore, if $j'(0) = 0$ and $l'(0) = 0$, then u small implies that p is also small and thus $\mathcal{A}(p)$ is coercive.*

Proof. The (formal) proof is very similar to that of Theorem 3.6. We introduce the Lagrangian defined for $(v,q) \in \big(H^1(\mathbb{R}^d;\mathbb{R}^d)\big)^2$ by

$$\begin{aligned} \mathcal{L}(\Omega,v,q) = & \int_\Omega j(v)\,dx + \int_{\partial\Omega} l(v)\,ds + \int_\Omega T(I+\nabla v)\cdot\nabla q\,dx - \int_\Omega q\cdot f\,dx \\ & - \int_{\Gamma_N} q\cdot g\,ds - \int_{\Gamma_D} \Big(q\cdot T(I+\nabla v)n + v\cdot T(I+\nabla q)n \Big) ds, \end{aligned}$$

And we investigate its stationarity conditions.

The partial derivative of $\mathcal{L}$ with respect to q, in the direction $\phi \in H^1(\mathbb{R}^d;\mathbb{R}^d)$,

after integration by parts, leads to

$$\begin{aligned}\langle\frac{\partial\mathcal{L}}{\partial q}(\Omega,u,p),\phi\rangle = 0 = \quad & -\int_\Omega \phi\cdot\Big(\mathrm{div}(T(I+\nabla u))+f\Big)dx \\ & +\int_{\Gamma_N}\phi\cdot\big(\big(T(I+\nabla u)\big)n-g\big)\,ds \\ & -\int_{\Gamma_D} u\cdot\big(\mathcal{A}(p)\nabla\phi\big)n\,ds.\end{aligned}$$

Taking first ϕ with compact support in Ω gives the state equation of (28). Then, varying the trace function ϕ on Γ_N gives the Neumann boundary condition for u, while varying the corresponding normal stress $\big(\mathcal{A}(p)\nabla\phi\big)n$ on Γ_D gives the Dirichlet boundary condition for u. (At this point we use the coercivity of $\mathcal{A}(p)$ which is a sufficient condition for $\big(\mathcal{A}(p)\nabla\phi\big)n$ to span a dense subset of $L^2(\Gamma_D)^d$.)

Then we differentiate $\mathcal{L}$ with respect to v in the direction $\phi\in H^1(\mathbb{R}^d;\mathbb{R}^d)$. This yields after integration by parts

$$\begin{aligned}\langle\frac{\partial\mathcal{L}}{\partial v}(\Omega,u,p),\phi\rangle = 0 = \quad & \int_\Omega\Big(j'(u)-\mathrm{div}(\mathcal{A}(u)\nabla p)\Big)\cdot\phi\,dx \\ & +\int_{\Gamma_N}\phi\cdot\Big(\big(\mathcal{A}(u)\nabla p\big)n+l'(u)\Big)\,ds \\ & +\int_{\Gamma_D}\Big(\phi\cdot\big(l'(u)+\mathcal{A}(u)\nabla pn-T(I+\nabla p)n\big) \\ & \qquad -p\cdot\big(\mathcal{A}(u)\nabla\phi\big)n\Big)ds.\end{aligned}$$

Taking first ϕ with compact support in Ω gives the adjoint state equation

$$-\mathrm{div}(\mathcal{A}(u)\nabla p) = -j'(u) \quad \text{in} \quad \Omega,$$

varying the trace of ϕ on Γ_N yields the Neumann boundary condition

$$\big(\mathcal{A}(u)\nabla p\big)n = -l'(u) \quad \text{on} \quad \Gamma_N,$$

then varying the normal stress $\big(\mathcal{A}(u)\nabla\phi\big)n$ with $\phi=0$ on Γ_D gives

$$p = 0 \quad \text{on} \quad \Gamma_D.$$

Finally, just like in the linear case, we have

$$J'(\Omega)(\theta) = \frac{\partial\mathcal{L}}{\partial\Omega}(\Omega,u,p)(\theta),$$

and the claimed expression of $J'(\Omega)(\theta)$ is obtained by applying Lemma 3.3 and 3.4 and remarking that $h=0$ on Γ_D. □

8.2 A numerical example

We come back to the medium cantilever problem described at the beginning of Section 6. The working domain is a rectangle of size 2×1 discretized with a rectangular 160×80 mesh, with zero displacement boundary condition on the left side and a downward vertical point load at the middle of the right side. The initialization is that of Figure 1 (middle). We use a Saint Venant-Kirchhoff material (see [18]) with a Young modulus equal to 1000 and a Poisson's coefficient equal to 0.3. This constitutive law is characterized by the following relations:

$$F = I + \nabla u, \quad E = \frac{1}{2}(F^T F - I),$$
$$\Sigma = \lambda \mathrm{Tr}(E) I + 2\mu E,$$
$$T(F) = F\,\Sigma.$$

This constitutive law does not satisfy any type of convexity (see Remark 8.1) so it is not clear that the elasticity equations (28) are well posed. Nevertheless, we follow the usual practice in structural optimization (see e.g. [12]) and adopt this Saint Venant-Kirchhoff law. The intensity of the force is now varying between 1 and 3, while the Lagrange multiplier for the weight constraint is adjusted to maintain a given global material proportion of 40% of the total volume. We first perform 10 iterations in the setting of linear elasticity to get a rough approximation of the shape, and then 100 in nonlinear elasticity. The resulting optimal shape in Figure 26 displays thicker bars under compression than under traction as it should be, the disymmetry being amplified by the intensity of the force.

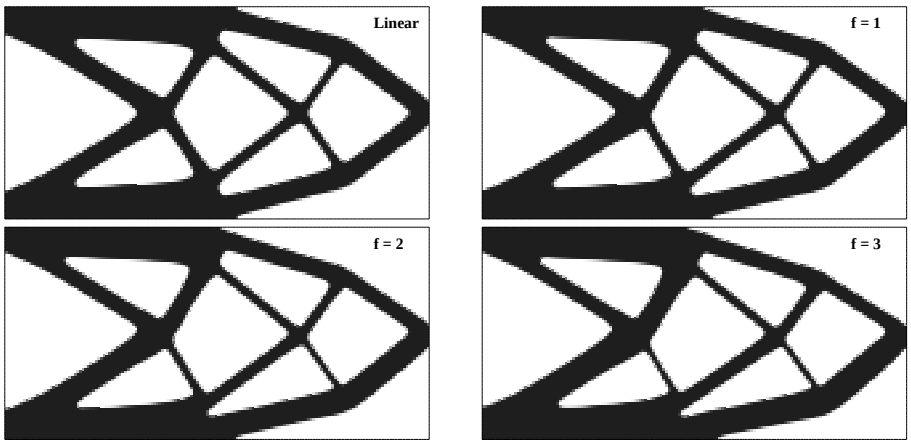

Figure 26: Optimal shape of a cantilever in nonlinear elasticity for different intensities of the force compared to the optimal shape in linear elasticity. Fine mesh (160×80), initialized as in Figure 1 (middle)

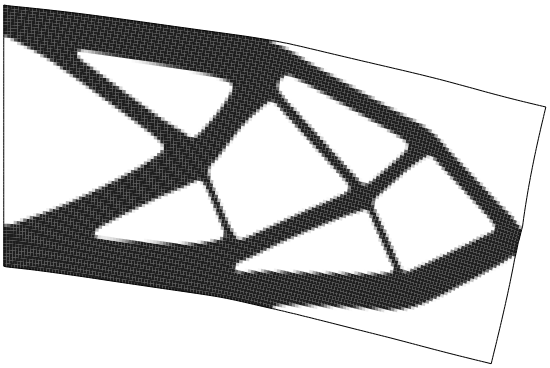

Figure 27: Deformed configuration for the optimal cantilever in nonlinear elasticity: the intensity of the force is 3 and the maximum displacement norm is equal to 0.4 (2×1 domain).

9 Conclusion

We have proposed a method for shape and topology optimization in two and three space dimensions which has the following advantages:

1. it allows for drastic topology changes during the optimization process ;
2. its cost is moderate in terms of CPU time since this is an Eulerian shape capturing method ;
3. it can handle very general objective functions and mechanical models, including nonlinear elasticity and design-dependent loads ;
4. with a good initialization it is as efficient as the homogenization method (when the latter one is available).

However, contrary to the homogenization method (see e.g. [1], [8], [17]), it is not a relaxation method, which means that local minima have not been fully eliminated in favor of global minima. It is clear from the numerical examples that there still exist local (and non-global) minima to which the method may converge if the initialization is too far from a global minimum. In practice, this level-set method behaves differently in 2-d and 3-d. In 2-d the method works as if it can reduce the topology (i.e. the number of holes) but it can not create new holes since there is no nucleation mechanism in our algorithm. Therefore, one must be careful in the choice of the initialization that should contain a large number of holes if one seek a non-trivial topology. In 3-d, there are less topological restrictions and the algorithm can easily create holes or non-simply connected shapes even if the initial guess is convex. The mechanism of 3-d topology changes is the possible crossing of two separate zero level-set surfaces without breaking the connectivity of the shape or of the void. Frequently the

final shape has a much more complex topology than the initial shape. Nevertheless, different initializations can still drive the algorithm to different optimal shapes in 3-d.

The problem of choosing an adequate initialization can be managed in two ways, at least. First, one can run the homogenization method on a simplified problem (say, linear elasticity with compliance objective function) as a preprocessor in order to find a correct initial topology. Second, one can couple our method with the so-called bubble method, or topological derivative, proposed by [19], [20], and [30], which is precisely a criteria for hole nucleation.

Finally, the present level-set method of shape and topology optimization can easily (in principle) be extended to multi-physics applications.

References

[1] Allaire G., *Shape optimization by the homogenization method, Springer Verlag, New York* (2001).

[2] Allaire G., Bonnetier E., Francfort G., Jouve F., Shape optimization by the homogenization method. *Nümerische Mathematik* **76**, 27-68 (1997).

[3] Allaire G., Jouve F., Optimal design of micro-mechanisms by the homogenization method, *European Journal of Finite Elements*, **11**, 405-416 (2002).

[4] Allaire G., Jouve F., Toader A.-M., A level-set method for shape optimization, *C. R. Acad. Sci. Paris, Série I*, **334**, 1125-1130 (2002).

[5] Allaire G., Kohn R.V., Optimal design for minimum weight and compliance in plane stress using extremal microstructures. *Europ. J. Mech. A/Solids* **12**, 6, 839-878 (1993).

[6] Ambrosio L., Buttazzo G., An optimal design problem with perimeter penalization, *Calc. Var.* **1**, 55-69 (1993).

[7] Ball J.M., Convexity conditions and existence theorems in nonlinear elasticity, *Archives for Rational Mechanics and Analysis,* **63**, 337-403 (1977).

[8] Bendsoe M., *Methods for optimization of structural topology, shape and material, Springer Verlag, New York* (1995).

[9] Bendsoe M., Kikuchi N., Generating Optimal Topologies in Structural Design Using a Homogenization Method. *Comp. Meth. Appl. Mech. Eng.* **71**, 197-224 (1988).

[10] Bendsoe M., Sigmund O., *Topology Optimization. Theory, Methods, and Applications*, Springer Verlag, New York (2003).

[11] Bourdin B., Chambolle A., Design-dependent loads in topology optimization. *ESAIM Control Optim. Calc. Var.* 9, 19-48 (2003).

[12] Buhl T., Pedersen C.B.W., Sigmund O., Stiffness design of geometrically nonlinear structures using topology optimization, *Structural and Multidisciplinary Optimization*, **19**, 2, 93-104 (2000).

[13] Chambolle A., A density result in two-dimensional linearized elasticity and applications. *Preprint CEREMADE* 121, Université Paris-Dauphine, 2001.

[14] Chambolle A., Larsen C.J., C^∞-regularity of the free boundary for a two-dimensional optimal compliance problem, *to appear in Calc. Var. Partial Diff. Eq.*.

[15] Céa J., Conception optimale ou identification de formes, calcul rapide de la dérivée directionnelle de la fonction coût, *Math. Model. Num. Anal.* **20**, 3, 371-402 (1986).

[16] Chenais D., On the existence of a solution in a domain identification problem, *J. Math. Anal. Appl.* **52**, 189-289 (1975).

[17] Cherkaev A., *Variational Methods for Structural Optimization,* Springer Verlag, New York (2000).

[18] Ciarlet P.G., *Mathematical Elasticity, Vol I : Three-Dimensional Elasticity,* North-Holland, Amsterdam (1988).

[19] Eschenauer H., Schumacher A., Bubble method for topology and shape optimization of structures, *Structural Optimization*, **8**, 42-51 (1994).

[20] Garreau S., Guillaume P., Masmoudi M., The topological asymptotic for PDE systems: the elasticity case. *SIAM J. Control Optim.* **39**, no. 6, 1756-1778 (2001).

[21] Mohammadi B., Pironneau O., *Applied shape optimization for fluids,* Clarendon Press, Oxford (2001).

[22] Murat F., Simon S., Etudes de problèmes d'optimal design. *Lecture Notes in Computer Science 41, 54-62, Springer Verlag, Berlin* (1976).

[23] Osher S., Santosa F., level-set methods for optimization problems involving geometry and constraints: frequencies of a two-density inhomogeneous drum. *J. Comp. Phys.*, **171**, 272-288 (2001).

[24] Osher S., Sethian J.A., Front propagating with curvature dependent speed: algorithms based on Hamilton-Jacobi formulations. *J. Comp. Phys.* **78**, 12-49 (1988).

[25] Pironneau O., *Optimal shape design for elliptic systems, Springer-Verlag, New York,* (1984).

[26] Sethian J.A., *Level-Set Methods and fast marching methods: evolving interfaces in computational geometry, fluid mechanics, computer vision and materials science,* Cambridge University Press (1999).

[27] Sethian J., Wiegmann A., Structural boundary design via level-set and immersed interface methods. *J. Comp. Phys.,* **163**, 489-528 (2000).

[28] Sigmund O., On the design of compliant mechanisms using topology optimization, *Mech. Struct. Mach.* **25**, 493-524 (1997).

[29] Simon J., Differentiation with respect to the domain in boundary value problems. *Num. Funct. Anal. Optimz.*, **2**, 649-687 (1980).

[30] Sokołowski J., Żochowski A., Topological derivatives of shape functionals for elasticity systems. *Mech. Structures Mach.* **29**, no. 3, 331-349 (2001).

[31] Sokołowski J., Zolesio J.P., *Introduction to shape optimization: shape sensitivity analysis, Springer Series in Computational Mathematics, Vol. 10, Springer, Berlin,* (1992).

[32] Wang M.Y., Wang X., Guo D., A level-set method for structural topology optimization, *Comput. Methods Appl. Mech. Engrg.*, **192**, 227-246 (2003).